Since January 2020 Elsevier has created a COVID-19 resource centre with free information in English and Mandarin on the novel coronavirus COVID-19. The COVID-19 resource centre is hosted on Elsevier Connect, the company's public news and information website.

Biochimie 146 (2018) 127–138

Contents lists available at ScienceDirect

Biochimie

journal homepage: www.elsevier.com/locate/biochi

Research paper

Chicken GRIFIN: Structural characterization in crystals and in solution

Federico M. Ruiz [a], Ulrich Gilles [b], Anna-Kristin Ludwig [c], Celia Sehad [d], Tze Chieh Shiao [d], Gabriel García Caballero [c], Herbert Kaltner [c], Ingo Lindner [b], René Roy [d, **], Dietmar Reusch [b, ***], Antonio Romero [a, ****], Hans-Joachim Gabius [c, *]

[a] Chemical and Physical Biology, Centro de Investigaciones Biológicas, CSIC, Ramiro de Maeztu 9, 28040 Madrid, Spain
[b] Pharma Biotech Development Penzberg, Roche Diagnostics GmbH, 82377 Penzberg, Germany
[c] Institute of Physiological Chemistry, Faculty of Veterinary Medicine, Ludwig-Maximilians-University, Veterinärstr. 13, 80539 Munich, Germany
[d] Pharmaqam and Nanoqam, Department of Chemistry, Université du Québec à Montréal, P.O. Box 8888, Succ. Centre-Ville, Montréal, Québec H3C 3P8, Canada

ARTICLE INFO

Article history:
Received 31 August 2017
Accepted 11 December 2017
Available online 15 December 2017

Keywords:
Aggregation
Crystallin
Galectin
Lectin
Lens
Ultracentrifugation

ABSTRACT

Despite its natural abundance in lenses of vertebrates the physiological function(s) of the galectin-related *inter-fiber protein* (GRIFIN) is (are) still unclear. The same holds true for the significance of the unique interspecies (fish/birds vs mammals) variability in the capacity to bind lactose. In solution, ultracentrifugation and small angle X-ray scattering (at concentrations up to 9 mg/mL) characterize the protein as compact and stable homodimer without evidence for aggregation. The crystal structure of chicken (C-) GRIFIN at seven pH values from 4.2 to 8.5 is reported, revealing compelling stability. Binding of lactose despite the Arg71Val deviation from the sequence signature of galectins matched the otherwise canonical contact pattern with thermodynamics of an enthalpically driven process. Upon lactose accommodation, the side chain of Arg50 is shifted for hydrogen bonding to the 3-hydroxyl of glucose. No evidence for a further ligand-dependent structural alteration was obtained in solution by measuring hydrogen/deuterium exchange mass spectrometrically in peptic fingerprints. The introduction of the Asn48Lys mutation, characteristic for mammalian GRIFINs that have lost lectin activity, lets labeled C-GRIFIN maintain capacity to stain tissue sections. Binding is no longer inhibitable by lactose, as seen for the wild-type protein. These results establish the basis for detailed structure-activity considerations and are a step to complete the structural description of all seven members of the galectin network in chicken.

1. Introduction

The emerging versatility of physiological functions of animal and human lectins gives ample reason to characterize their structures in detail. In overview, more than 12 folds have been identified that convey ability to bind glycans [1–4]. Sequence divergence after duplication events, starting from an ancestral gene, then led to forming families of homologous proteins. The case study on galectins (β-galactoside-binding proteins with β-sandwich fold and a sequence signature responsible for ligand contact [5]) is describing such a network with overlapping and distinct expression profiles [6–8]. This emerging evidence poses the challenge of a complete characterization of the galectins of an organism. It would be a step forward towards delineating rules of network design and providing insights into the functional meaning of sequence variations. In this respect, the galectin fold presents remarkable adaptability for accommodating ligands of different biochemical nature.

The crystallographic or NMR spectroscopical study of such domains of protozoan (*Toxoplasma gondii*) micronemal protein 1 and

Abbreviations: Å, Ångström; Arg, arginine; Asn, asparagine; Asp, aspartate; CG, chicken galectin; C-GRIFIN, chicken galectin-related *inter-fiber protein*; Gln, glutamine; Glu, glutamate; HDX, hydrogen/deuterium exchange; His, histidine; ITC, isothermal titration calorimetry; Leu, leucine; Lys, lysine; SAXS, small angle X-ray scattering; Trp, tryptophan; Val, valine.

* Corresponding author.
** Corresponding author.
*** Corresponding author.
**** Corresponding author.
E-mail addresses: roy.rene@uqam.ca (R. Roy), dietmar.reusch@roche.com (D. Reusch), romero@cib.csic.es (A. Romero), gabius@tiph.vetmed.uni-muenchen.de, gabius@lectins.de (H.-J. Gabius).

https://doi.org/10.1016/j.biochi.2017.12.003
0300-9084/

protein 2-associated protein [9,10] as well as the N-terminal modules of bovine and murine coronavirus spike proteins [11,12] have taught the following instructive lesson: conversion of the concave topology of the carbohydrate-binding pocket established by surrounding loops to a predominantly hydrophobic surface shifts specificity from glycans to distinct proteins. Looking at the assumedly crucial sequence signature for contact to a β-galactoside, a less dramatic deviation than just described may not necessarily impair glycan binding. For example, the change of a seemingly essential Asn (in position 46 in human galectin-1 (Gal-1)) to Ala at the equivalent position 64 in a fungal (*Agrocybe cylindracea*) galectin is not detrimental. It is neutralized by a five residue insertion at positions 42–46 (with the inserted Asn46 taking the place of the Asn lost at position 64) [13,14]. The structural way how to maintain affinity for lactosides in the conger eel (*Conger myriaster*) galectin from peritoneal cells (Con-P), although even seven from eight conserved amino acids are replaced as reported in [15], has not yet been characterized. Alternatively, sequence deviation(s) can alter carbohydrate specificity. The Trp81Arg change implemented binding to bi-N-acetylated disaccharides (chitobiose, LacdiNAc) in the third galectin protein (CGL3) from the inky cap mushroom *Coprinopsis cinerea* [16]. A unique situation, i.e. a species-dependent loss of lectin activity, is encountered for the galectin-related *i*nter-*f*iber prote*in*, termed GRIFIN.

This protein has first been described in rat as lens-specific protein [17,18]. It was found in the insoluble fraction of nuclear fiber cells and localized at the interface between adjacent fiber cells, representing about 0.5% of total protein in adult lens. Its gene with an elaborate promoter region to facilitate lens-specific expression is a common constituent of vertebrate genomes [19]. Given this site-specific occurrence and conserved presence among vertebrates, it is exceptional and thus intriguing to see sequence deviations at canonical positions between mammalian and bird/fish GRIFINs. Especially, the equivalent of the already noted Asn46 (in human Gal-1) is turned to Lys in mammalian GRIFINs [17]. As consequence, a bead (lactosylated Sepharose beads) assay revealed no lectin activity for rat GRIFIN [17]. In contrast, GRIFINs from zebrafish [20] and chicken [19] were bona fide lectins. Two reasons prompted us to initiate structural analysis of GRIFINs by studying chicken (C)-GRIFIN: the mentioned plasticity within the galectin fold and our long-term interest to achieve complete crystallographic documentation of galectin structures in an organism. Towards this end, chicken with its (only) seven family members is a favorable model. Since C-GRIFIN shares a deviation from the canonical sequence for lactose binding with mammalian GRIFINs, i.e. the Arg71Val exchange, defining the resulting contact pattern to the ligand will enable a comparison to common features. We here combine crystallographical analysis, reaching atomic resolution, with studies of C-GRIFIN in solution. They were started by determining its quaternary structure, a key feature of proto-type galectin functionality [21].

Quaternary structure and tendency for aggregation were first examined in solution, up to a concentration of 9 mg/mL, by ultracentrifugation and small angle X-ray scattering (SAXS). Crystallographically, respective specimen from solutions at seven pH values ranging from 4.2 to 8.5 could be processed to monitor stability of structural features. The interaction with lactose was monitored in the crystals and also in solution. Here, thermodynamic parameters (by isothermal titration calorimetry (ITC)) and profiles of hydrogen/deuterium exchange (HDX) in the absence and presence of the ligand were measured. Faced with the conundrum that re-establishing the sequence signature in rat GRIFIN with the Lys-to-Asn reconstitution did not repair the loss of lectin activity [17], we finally probed into the effects of site-specific mutations on C-GRIFIN's carbohydrate-binding activity by a histochemical assay.

2. Material and methods

2.1. Protein production

The wild-type protein was obtained after recombinant production directed by a pGEMEX-1 vector with the respective cDNA insert and purified by affinity chromatography using lactose-bearing resin as described [19]. cDNAs of the mutants of C-GRIFIN, i.e. the Trp66Lys and the Asn48Lys single-site mutants, the Asn48Lys/Arg50Val double mutant and the Asn48Lys/Arg50Val/Tyr66Leu triple mutant, were prepared by using the QuikChange™ Site-Directed Mutagenesis protocol (Agilent Technologies, Munich, Germany). The following primer pairs were used: 5′ C CTG GCC AAC CAC CTG GGG AAG GAG GAG G 3′ and 5′ C CTC CTC CTT CCC CAG GTG GTT GGC CAG G 3′ (Trp66Leu), 5′ C GCC TTC CAC TT T AAG CCC CGC TTT GCC AGC 3′ and 5′ GCT GGC AAA GCG GGG CTT AAA GTG GAA GGC G 3′ (Asn48Lys), 5′ GCT GGC AAA GAC GGG CTT AAA GTG GAA GGC G 3′ and 5′ C GCC TTC CAC TTT AAG CCC GTC TTT GCC AGC 3′ (Asn48Lys/Arg50Val) (exchanged base pairs are underlined). The cDNA of the triple mutant was generated by further altering the cDNA of the double mutant (Asn48Lys/Arg50Val) by respective processing with the primers for the Trp66Leu mutant. Successful implementation of the intended changes was checked by DNA sequencing (Sequiserve, Vaterstetten, Germany).

Mutant proteins of C-GRIFIN were designed as fusion proteins with a glutathione S-transferase (GST) part in a pGEX-6p-2 vector (GE Healthcare, München, Germany), they were purified after recombinant production by affinity chromatography using glutathione-presenting Sepharose 4B (GE Healthcare). Thereafter, the linkage between both proteins was cleaved by GST-tagged human rhinovirus 3C protease (at a ratio of 1:100 (w/w)), then the C-GRIFIN part was separated from released GST and the tagged protease by a second round of affinity chromatography as described [19]. Protein was either precipitated by adding $(NH_4)_2SO_4$ or labeled by biotinylation for the histochemical analysis, as described for human Gal-1 [22].

2.2. Analytical ultracentrifugation

Protein samples were diluted to final concentrations of 0.5 and 1.0 mg/mL in 5 mM phosphate buffer containing 150 mM NaCl and 4 mM β-mercaptoethanol, and solutions were pre-cleared at 16,000 × g. Sedimentation-velocity experiments were run at 293 K in an Optima KL-I analytical ultracentrifuge (Beckman Coulter, Indianapolis, USA) with an An50-Ti rotor and standard double-sector Epon-charcoal center pieces (1.2 cm optical path length). Measurements were performed at 48,000 rpm, registering the course of protein migration every minute at 280 nm. Rayleigh interferometric detection was used to monitor the course of development of the concentration gradient as a function of time and radial position, and the data were analyzed using the SedFit software (Version 14.7).

2.3. Small angle X-ray scattering (SAXS)

SAXS data were collected at the BM29 beamline (ESRF Synchrotron, Grenoble, France) using the BioSAXS robot and a Pilatus 1 M detector (Dectris, Baden-Daettwill, Switzerland) with synchrotron radiation at a wavelength of $\lambda = 1.0$ Å and a sample-detector distance of 2.867 m [23]. Each measurement consisted of 10 frames, each of 1 s exposure of a 100 μL sample flowing continuously through a 1 mm diameter capillary during exposure to X-rays. Buffer scattering was measured immediately before each measurement of the corresponding protein sample at 277 K. The obtained scattering profiles were spherically averaged, and the

buffer scattering intensities were subtracted using in-house software. Protein samples were prepared at concentrations of 1, 2, and 9 mg/mL in 20 mM phosphate buffer (pH 7.0) containing 150 mM NaCl and 5 mM lactose. Particle envelopes were generated ab initio using the program DAMMIF [24]. Multiple runs were performed to generate 30 independent model shapes that were combined and filtered to produce an averaged model using the DAMAVER software package [25].

2.4. Crystallization, data collection and processing

Suspensions of precipitated protein were extensively dialyzed against 5 mM phosphate buffer (pH 7.0) containing 150 mM NaCl and 4 mM β-mercaptoethanol. Protein was purified by affinity chromatography using a column packed with lactosylated Sepharose 4B to remove inactive material. Fractions after elution with 200 mM lactose were concentrated using Amicon Ultra 10,000 MCWO centrifugal filter units and then loaded on a HiPrep 16/60 Sephacryl S-200 column equilibrated with phosphate-buffered saline (pH 7.0) containing 4 mM β-mercaptoethanol and 5 mM lactose. The protein eluted as a single peak, the respective fractions were concentrated to a concentration of 15 mg/mL. Separately, protein was purified in the absence of lactose by loading sample directly after dialysis on a gel filtration column as above equilibrated with phosphate-buffered saline (pH 7.0) containing 4 mM β-mercaptoethanol. Eluted protein fractions were finally concentrated as described above.

Crystallization was performed at 295 K using the sitting-drop vapour diffusion method. Small crystals appeared in a wide range of crystallization conditions. In detail, crystal size and quality were optimal at the following conditions: 20% PEG 8000, 0.1 M phosphate/citrate (pH 4.2); 30% PEG 4000, 0.1 M sodium acetate (pH 4.6), 0.2 M ammonium sulfate; 20% PEG 1000, 0.1 M phosphate (pH 6.2), 0.2 M NaCl; 30% PEG 400, 0.1 M MES (pH 6.5), 0.1 M sodium acetate; 5% (w/v) 2-propanol, 0.1 M Hepes (pH 7.5); 10% PEG 3000, 0.1 M imidazole (pH 8.0), 0.2 M Li_2SO_4; 20% (v/v) methanol, 0.1 M Tris (pH 8.5), 0.01 M $CaCl_2$.

Each crystal was flash-cooled by immersion in liquid nitrogen using the corresponding crystallization medium supplemented with 30% ethylene glycol as cryo-solution. All data collections were done at the XALOC beamline of the ALBA synchrotron (Cerdanyola del Vallès, Spain) except for the crystal obtained at pH 4.6 that was taken to the Proxima 2 beamline of the SOLEIL synchrotron (Gif-sur-Yvette, France). Diffraction data were processed using XDS [26] and Aimless [27]. A summary of reflection data parameters is presented in Table 1.

2.5. Structure determination and refinement

The molecular replacement method was used to solve C-GRIFIN's structures, using the program Phaser from the Phenix suite [28]. A theoretical model generated by the Swiss-Model Server (http://swissmodel.expasy.org) was applied as a search probe [29]. The Phenix suite [28] was employed for structural refinements, and addition of water molecules and placement of lactose were carried out manually with the Coot program [30], if necessary. The statistical details of final models are given in Table 1. Molecular illustrations of the structural models were generated using Pymol.

2.6. Isothermal titration calorimetry

Solutions of C-GRIFIN (5 μM or 200 μM (at pH 8.5)) were prepared in phosphate-buffered saline (10 mM, pH 7.2), in Tris-HCl (30 mM, pH 8.5) or in sodium acetate (10 mM, pH 5.2). The ligand-containing solutions (100 μM or 60 mM (at pH 8.5) for β-lactosides, 40 μM for the 3′-O-sulfated derivative of the 2-naphthyl β-lactoside) were also freshly prepared just before starting the experiment by injecting first 2 μL, then 10 μL (or 5 μL for the titration at pH 8.5) of ligand-containing solution into the cell of a Microcal VP-ITC calorimeter (GE Healthcare), filled with the protein-containing solution, at 298 K. Control experiments using buffer excluded lectin-independent heat generation. Resulting data were fitted using the Origin software package.

2.7. Sample preparation for HDX–LCMS analysis

A solution of lactose and C-GRIFIN at a molar ratio of 2344:1 in equilibration buffer (20 mM potassium phosphate containing 97 mM sodium chloride in H_2O, pH 7.5), with a lactose-free solution as control, was incubated for 1 h at room temperature. HDX was started at room temperature by adding 10-times deuteration buffer (20 mM potassium phosphate containing 97 mM sodium chloride in D_2O, pD 7.9, pH 7.5) to each sample. After 0.5 min, 1 min, 10 min, 30 min, 60 min and 240 min, the deuterated samples were quenched by adding ice-cold quenching buffer (100 mM potassium phosphate buffer containing 5 M guanidinium chloride and 0.5 M Tris[2-carboxyethyl]phosphine hydrochloride in H_2O, pH 2.4) at a 1:1 ratio, followed by immediate freezing on dry ice, as previously performed for the N-terminal lectin domain of chicken galectin (CG)-8, referred to as CG-8N [31]. In parallel, protein solutions without lactose were kept in equilibration buffer without deuteration and quenched in the same way, this undeurated control sample used for identification of the peptic peptides. Experiments were performed in triplicate.

2.8. HDX-LCMS analysis

Quenched undeuterated and deuterated sample solutions (320 pmol C-GRIFIN) were injected into a nanoAcquity UPLC system with HDX technology (Waters Corporation, Milford, USA), allowing an online peptic digest on a Poroszyme-presenting pepsin cartridge (2.1 mm × 30 mm; Applied Biosystems, Foster City, USA) at 15 °C. Peptic peptides were then trapped on an Acquity UPLC BEH C18 VanGuard pre-column (1.7 μm, 2.1 mm × 5 mm; Waters) and separated with a linear acetonitrile gradient over 14 min at 0 °C on an Acquity UPLC BEH C18 column (1.7 mm, 1 mm × 100 mm; Waters). The column outlet was directly connected to a Synapt G2 HDMS mass spectrometer equipped with a lockspray ESI source (Waters). Mass spectra for the peptic peptides were acquired in the MSE mode over the range of m/z 50–2000.

2.9. Data analysis

Identified peptic peptides obtained by the digestion of C-GRIFIN were organized as list using the Protein Lynx Global Server software (Waters) and the MSE data for the undeuterated controls. By applying DynamX software (Waters), the relative deuterium uptake for each identified peptide was calculated by subtracting the centroid masses of the corresponding peptides found in the undeuterated and deuterated samples, for both ligand-loaded and ligand-free C-GRIFIN. The ligand-dependent difference in relative deuterium uptake was determined using DynamX, and its significance was evaluated by calculating a two-sided confidence limit with a significance level of 0.02 [32]. The result of this evaluation was visualized by color coding of β-strands in the three-dimensional model of C-GRIFIN.

2.10. C-GRIFIN histochemistry

Biotinylated C-GRIFIN and its Asn48Lys, Trp66Leu, Asn48Lys/

Table 1
Data collection and refinement statistics for C-GRIFIN structures.

Crystallization condition	pH 4.2, 1.1 M phosphate-citrate, 20% PEG 8 K, 0.2 M NaCl	pH 4.6, 0.1 M acetate, 30% PEG 4 K, 0.2 M $(NH_4)_2SO_4$	pH 6.2, 0.1 M phosphate, 20% PEG 1 K, 0.2 M NaCl	pH 6.5, 0.1 M MES/acetate, 30% PEG 400	pH 7.5, 1.1 M HEPES, 5% (w/v) 2-propanol	pH 8.0, 1.1 M imidazole, 10% PEG 3 K, 0.2 M Li_2SO_4	pH 8.5, 1.1 M Tris/HCl, 20% (w/v) MetOH, 0.01 M $CaCl_2$
unit cell content (chains)	2	2	4	1	2	4	1
resolution range (Å)	39.05–1.15 (1.19–1.15)	40.26–1.46 (1.51–1.46)	48.22–2.10 (2.17–2.10)	40.39–1.40 (1.45–1.40)	39.11–0.96 (0.99–0.96)	35.21–1.84 (1.91–1.84)	36.11–1.10 (1.14–1.10)
space group	P 1 21 1	P 1 21 1	P 2 21 21	P 42 21 2	P 1 21 1	P 2 21 21	P 42 21 2
unit cell	39.09 60.8 53.99 90 92.6 90	38.94 60.27 54.14 90 92.5 90	44.87 103.93 129.42 90 90 90	80.77 80.77 39.15 90 90 90	39.14 60.73 53.87 90 92.4 90	45.63 103.97 130.78 90 90 90	80.74 80.74 39.23 90 90 90
total reflections	136742 (10596)	72017 (6297)	69784 (5905)	52082 (4979)	279031 (23887)	108573 (10375)	105180 (9372)
unique reflections	85844 (7759)	39758 (3661)	35607 (3189)	26072 (2502)	148722 (13666)	54344 (5238)	52748 (4826)
multiplicity	1.6 (1.4)	1.8 (1.7)	2.0 (1.9)	2.0 (2.0)	1.9 (1.7)	2.0 (2.0)	2.0 (1.9)
completeness (%)	95.61 (86.82)	90.98 (84.47)	98.20 (89.81)	99.72 (98.08)	97.04 (89.78)	99.75 (97.92)	99.14 (92.12)
mean I/sigma (I)	12.53 (2.14)	15.18 (1.02)	13.72 (1.24)	14.45 (1.36)	15.02 (2.41)	14.12 (1.66)	14.33 (1.64)
Wilson B-factor	10.26	13.75	37.52	13.20	8.06	31.56	9.07
R-merge	0.024 (0.28)	0.093 (0.56)	0.048 (0.47)	0.029 (0.53)	0.023 (0.30)	0.021 (0.47)	0.026 (0.45)
R-meas	0.035	0.132	0.068	0.041	0.033	0.030	0.037
CC1/2	0.99 (0.82)	0.97 (0.48)	0.99 (0.67)	0.99 (0.59)	0.99 (0.82)	1 (0.63)	1 (0.63)
CC*	1 (0.95)	0.99 (0.81)	0.99 (0.89)	1 (0.86)	1 (0.95)	1 (0.88)	1 (0.88)
R-work	0.14 (0.22)	0.17 (0.31)	0.21 (0.32)	0.16 (0.29)	0.13 (0.21)	0.18 (0.26)	0.13 (0.25)
R-free	0.16 (0.23)	0.22 (0.33)	0.28 (0.39)	0.20 (0.31)	0.15 (0.21)	0.22 (0.29)	0.15 (0.28)
number of non-hydrogen atoms	2652	2611	4755	1340	2644	4966	1400
macro-molecules	2327	2307	4479	1147	2325	4527	1201
ligands			92	23	23	92	23
water	325	304	184	170	296	347	176
protein residues	274	275	544	136	274	547	137
RMS (bonds)	0.008	0.006	0.007	0.005	0.009	0.008	0.009
RMS (angles)	1.04	0.86	0.92	0.81	1.49	1.17	1.44
Ramachandran favored (%)	97	96	95	96	97	96	97
Ramachandran outliers (%)	0.74	0.74	1.1	0.7	0.7	0.73	0.66
clashscore	2.80	3.27	10.53	3.87	3.23	6.68	2.83
average B-factor	14.50	16.96	41.86	17.49	11.30	36.20	12.10
macro-molecules	12.70	15.57	41.61	15.39	9.70	35.60	10.10
ligands			47.42	21.72	10.60	40.60	15.60
solvent	27.48	27.54	45.02	31.08	23.90	43.00	25.50
PDB code	5NLZ	5NM6	5NM1	5NMJ	5NLD	5NLE	5NLH

Statistics for the highest-resolution shell are shown in parentheses.

Arg50Val and Asn48Lys/Arg50Val/Trp66Leu mutants were tested on paraffin-embedded sections (5 μm) of adult chicken kidney, obtained after fixation of tissue specimens for 24 h in Bouin's solution and embedded, mounted on Superfrost® Plus glass slides (Menzel, Braunschweig, Germany). Following optimized processing for deparaffinizing sections, blocking of sites for non-specific binding, incubation of biotinylated probe in the absence and presence of lactose (200 mM) and signal development by bound avidin-alkaline phosphatase (AP) conjugate with Vector® Red AP substrate (Enzo Life Sciences, Lörrach, Germany) as described [33,34], documentation was recorded using an AxioImager.M1 microscope (Carl Zeiss MicroImaging, Göttingen, Germany) equipped with an AxioCam MRc3 and MRc digital camera and AxioVision (version 4.6) software. Processing controls with an incubation step using plain buffer instead of buffer containing the labeled probe excluded probe-independent staining, titrations with probe concentrations of 4 μg/mL, 12 μg/mL, 24 μg/mL and 48 μg/mL were systematically performed for all proteins and for the pair of measurements in the absence and presence of lactose.

3. Results and discussion

3.1. Quaternary structure in solution

At low concentrations in the course of gel filtration, GRIFINs from chicken, mouse and rat eluted at the position of a dimer, with evidence for inter-subunit exchange when fractionating mixtures of tag-free and tagged proteins [17,19,35]. Considering the high local concentration in the lens, we examined the protein status after further increasing the concentration. In sedimentation-velocity experiments at concentrations up to 1.0 mg/mL, C-GRIFIN migrated as single sharp peak with a sedimentation coefficient of 2.6 ± 0.1 S. In comparison, homodimeric human Gal-1 and CG-1A gave very similar values under these conditions, whereas CG-2 has an S-value of 2.03 ± 0.1 [36]. Frictional ratios among homodimeric proto-type CGs can thus differ when measured by ultracentrifugation. It is about 1.3 for C-GRIFIN and CG-1A but 1.63 for CG-2 [36]. Of note for CG-2, heterogeneity in size distribution had been observed for this protein at 4 mg/mL, with the acquisition of the quaternary structure as trimer of dimers [37]. We proceeded to

determine the quaternary structure of C-GRIFIN at concentrations up to 9.0 mg/mL. When reaching the concentration of 9.0 mg/mL in SAXS experiments, the particle distribution function of C-GRIFIN is still in agreement with exclusive presence of a dimer. The ab initio model of the dimer calculated with these data is shown in Fig. 1. Its elongated disc shape fits well with the frictional ratio of the dimer as calculated using data obtained by ultracentrifugation. Overall, no evidence for aggregation up to this concentration was obtained. These results thus define the quaternary structure in solution as homodimer with no indication for higher-order aggregates at concentrations up to 9 mg/mL under the given conditions. Structural analysis was next taken to the level of crystallography.

3.2. Crystallographic structure: global aspects and interface

In view of the remarkable long-term stability of C-GRIFIN in lenses, it was attempted to prepare a panel of crystals from solutions over a broad pH range. A wide range of combinations of buffers and additives was tested and structural analysis became possible with crystals obtained at seven conditions. In addition to presence of different types of additives, they covered the pH range from 4.2 to 8.5. As summarized in Table 1, the resolution reached the level of 0.96 Å for crystals grown at pH 7.5. Space groups differed within this group, $P21$ seen in three cases, either $P4_22_2$ or $P22_12_1$ in two cases. The asymmetric unit cell content was variable in the seven crystals, being either one, two or four (Table 1), and Fig. S1 presents representative illustrations obtained for each crystal (at pH values of 7.5, 8.0, 8.5, 6.5, 6.2, 4.6 and 4.2).

The C-GRIFIN monomer adopts the typical β-sandwich fold with two anti-parallel β-sheets of six (S1-S6) and five (F1-F5) β-strands (Fig. 2). The short 3_{10} helix in the long loop connecting the S2/F5 strands is also a typical feature. Among the proto-type CGs [37–39], the loop between the S3/S4 strands reaches the largest length, as highlighted by rectangles in Fig. 3. Loop-length variation also holds true for the S4-S5 section. It is four amino acids shorter than in CG-1A/B, while superimposing with that of CG-2 (Fig. 3). As consequence, a flat surface is created in this region (Fig. 3). Length, conformation and structure of this loop has been described as a discriminatory factor between human Gal-1 and -3 when interacting with the TF antigen [40], the core 1 disaccharide of mucin-type O-glycosylation (CD176) [41]. Overall, alignment is at a high level, as reflected by rmsd values at 2.9 Å (to CG-1A, CG-2) and 2.1 Å (CG-1B). For comparison, respective values are 2.4 Å for CG-1A/CG-2 and 1.5 Å for the paralogue pair CG-1A/B.

The availability of crystals of C-GRIFIN exposed to a wide range of pH values enabled a detailed comparison of the seven crystal structures. It revealed no marked structural changes, the common homodimer shown in Fig. 4A. To substantiate this conclusion by a number, the rmsd value was 0.337 Å for the pairwise analysis of the

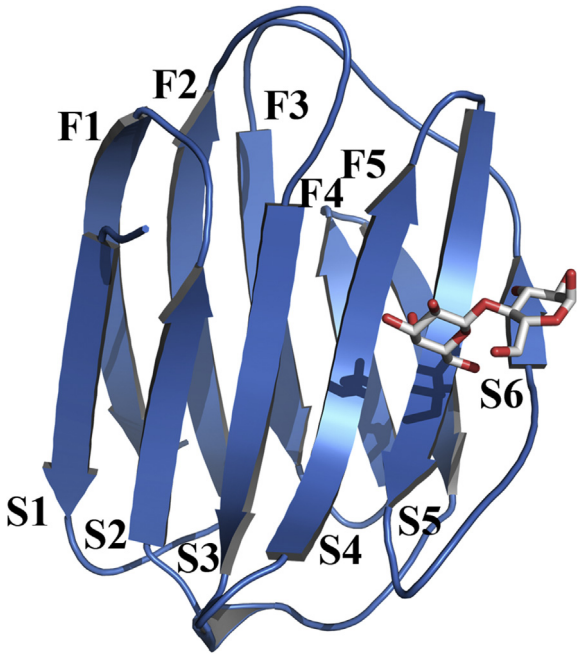

Fig. 2. Monomer structure of C-GRIFIN with the typical β-sandwich fold and contact site for lactose.

crystal structures at the tested pH minimum (4.2) and its maximum (8.5). Since the availability of the crystallographic homodimer structure made its placement into the sphere of the SAXS-derived model possible, as done in Fig. 1, the fitting of crystal and solution structures could be tested and was found to be excellent.

Looking at the unit cell content of the seven crystals, it differs considerably, as indicated in Table 1. The example of CG-2, which is arranged as a non-crystallographic trimer of dimers (added to Fig. S1) and occurs in part as hexamer in solution at 4 mg/mL in sedimentation-velocity analysis, underlines capacity of homodimer association of a galectin [13]. Crystal packing of other galectins to a dimer of dimers [42,43], also seen for human Gal-1 in solution in an aprotic solvent [44], that can even be stable in solution [16,45–47] as well as the aggregation of a monomer (murine Gal-9N) to a dimer [48] and Na^+-mediated association of the N-terminal lectin domain of murine Gal-4 to a tetramer around the crystallographic four-fold axis [49] indicate potential of galectin domains for building higher-order aggregates under special conditions. In this study, the availability of crystals of the same protein obtained at different conditions documents the very low degree of influence of the pH value on the galectin fold, with some variability in unit cell

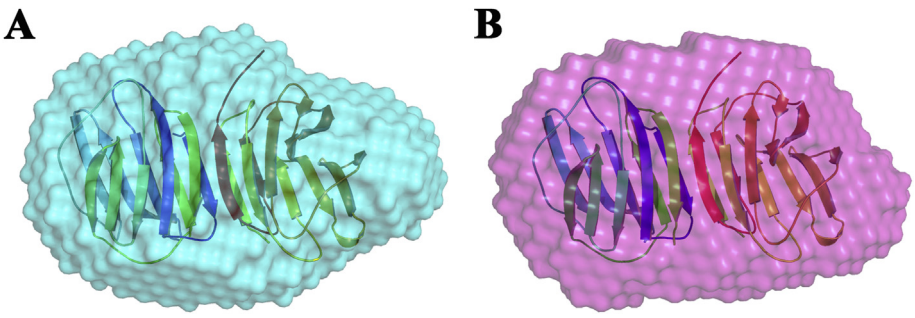

Fig. 1. Ab initio SAXS-based models of lactose-free (A) and lactose-loaded (B) C-GRIFIN. The shape of an elongated disc can readily accommodate the crystallographic structure (please see Fig. 4A) and fits well to the frictional ratio determined by sedimentation-velocity experiments.

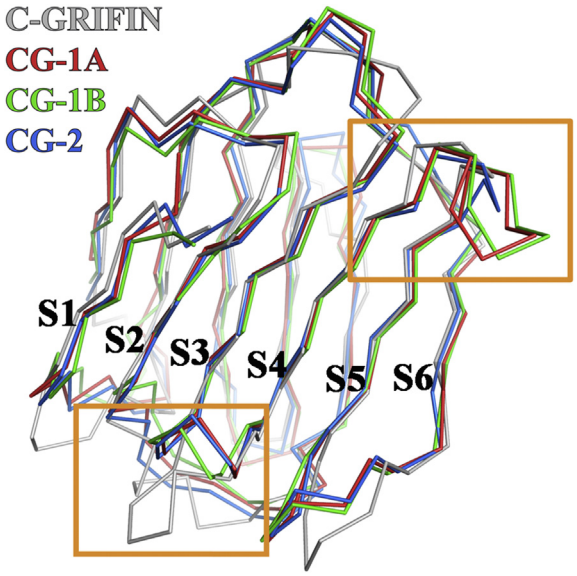

Fig. 3. Topological alignment of the crystal structures of C-GRIFIN (grey), CG-1A (red), CG-1B (green) and CG-2 (blue). Regions of structural differences in loops are highlighted with orange squares.

content.

Looking closely at the interface region between the two subunits of C-GRIFIN's homodimer, it is established by the F1/S1 strands from the N- and C-termini of each subunit in the homodimer (residues 4–14/127-136) (Fig. 4B). Around the S1 edge, the salt bridge between Arg5/Glu12 and hydrogen bonds between Glu7/Leu9 stabilize the assembly. In the case of the anti-parallel F1 strands, hydrogen bonding between Ser131/Thr135 and also Ser130, Ile134 and Lys136 serve this purpose. Typically for CG homodimers, hydrophobic contacts via Phe6, Ile129, Val132 and Ile134 come into play, too (Fig. 4B). Together, these contacts enable C-GRIFIN to act as cross-linker, reported previously based on haemagglutination assays [19], or as a kind of molecular glue (please see below). The susceptibility to abolish the cell bridging by presence of lactose at 1.0–1.5 mM, together with C-GRIFIN's binding to lactose-bearing beads used in affinity chromatography, was indicative of lectin activity. Here, we first confirm this conclusion by ITC analysis and then characterize the contact site and its pattern of contact formation with lactose crystallographically.

3.3. Thermodynamics of binding of lactose by C-GRIFIN

Analysis of ITC data for the association of C-GRIFIN and the β-methyl derivative of lactose resulted in revealing this process to be enthalpically driven. Homodimeric CG-1A and CG-2 had similar thermodynamics of binding, whereas ligand association to CG-1B produced a relatively small enthalpy gain [13]. Per dimer, the number of binding sites of 1.76 ± 0.42 was reached at pH 7.2. It increased to 1.89 ± 0.45 by exchanging the methyl by a 2′-naphthyl group, together with the considerable enhancement of affinity from 140 μM to 8.6 μM. Adjusting the pH to 8.5 (in TRIS buffer) lowered ligand loading to well below 1 and also the affinity. At the acidic side, no heat production was observed at pH 5.2 (in sodium acetate). This pH profile with rather sharp decreases in binding activity to both sides corresponded well with assays on human Gal-1 using lactose-bearing beads or surface-immobilized asialofetuin [50,51]. Fittingly, binding sites for lactose in the homodimer were occupied by the ligand in the crystals obtained at pH values of 6.2, 6.5, 8.0 and 8.5, and they remained free when the pH was set to 4.2/4.6. Interestingly, a special circumstance precluded complete loading of both sites of the homodimer at pH 7.5 in the crystal.

3.4. Crystallographic structure: carbohydrate-binding site

At this pH value, crystallographic contacts with Asn28 of a symmetry-related subunit impedes access to one lactose-binding site of the homodimer. This situation makes a comparison of lactose-free with lactose-loaded subunits possible at atomic resolution. The resulting rmsd value of this superimposition is 0.263 Å, arguing in favor of a common shape irrespective ligand loading. The contact site in crystals at each pH value is composed of amino acids from β-strands S4-S6 (Fig. 4A). Interestingly, the electron density map of the ligand shows a preference for presence of α-lactose instead of the natural β-anomer at the reducing end, as shown in Fig. S2, likely by crystallographic contacts. Despite sequence variations among the homodimeric CGs, the canonical contact profile between the protein and lactose is maintained, except for the Arg71Val substitution (Fig. 5). As illustrated in this figure, the axial 4′-hydroxyl group of the galactose moiety is involved in hydrogen (H-)bonding with the conserved His46, Asn48 and Arg50 moieties, sequence conservation of Asn59/Glu69 enabling H-bonding with the 6′-hydroxyl group. In addition, the 3′-hydroxyl is in water-mediated contact with Glu32, and C-H/π interactions with Trp66 complete the binding pattern for the galactose moiety. Since Trp oxidation to the oxindole impairs ligand binding, as first shown for electrolectin [52], the substantial reactivity of this residue (up to 18.6% after 24 h when exposed to 0.05% hydrogen peroxide [19]) is noteworthy. Deamidation within peptide 58–70 (after seven days at 25 °C/40 °C reaching 9.2%/13.5% [19]) may also have an impact on the protein's lectin activity, if not protected by bound ligand.

In addition to galactose, the 3′-hydroxyl group of the glucose

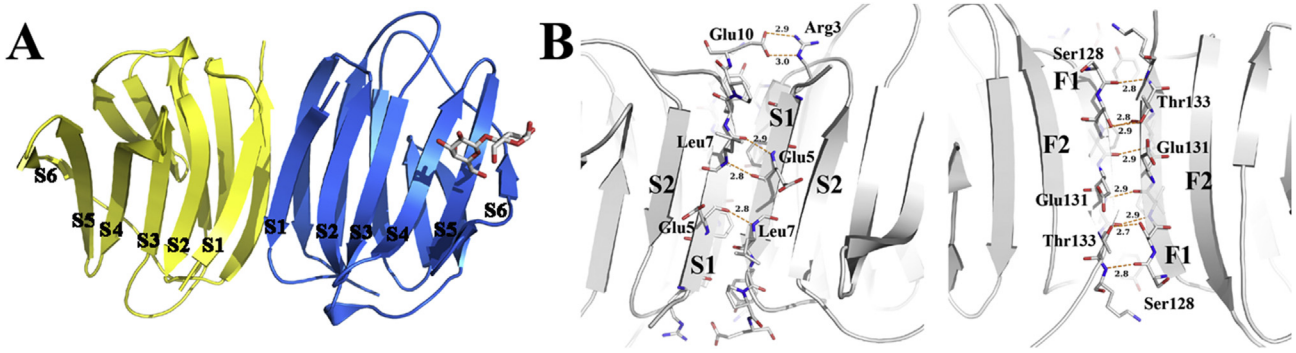

Fig. 4. Overview on the structure of the C-GRIFIN homodimer (A) and the profile of hydrogen bonding in the interface (B), distances given in Å.

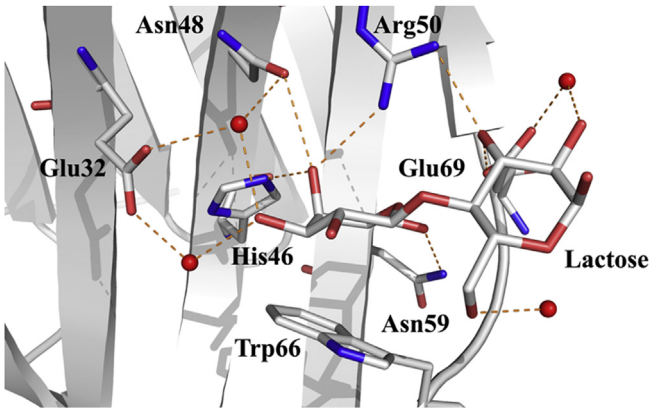

Fig. 5. Illustration of the contacts between lactose and amino acids in the carbohydrate-binding site of C-GRIFIN.

part of lactose contributes to ligand binding, as shown for CG-1A and CG-2 by measuring inhibitory capacity of methyl β-lactosides on lectin binding to asialofibrin [53]. β-Methyl derivatives of lactose with 3-deoxy and 3-deoxy-3-methyl glucose have low or no inhibitory potency on CG-1A (and human Gal-1). In C-GRIFIN, this 3-hydroxyl connects by H-bonding with Arg50 and Glu69 (Fig. 5). Val71, taking the place of the Arg residue conserved in homodimeric CGs and zebrafish GRIFIN, is not able to engage in H-bonding. When for example compared to CG-2 [13], the Arg71Val substitution causes a loss in H bonding to this hydroxyl for C-GRIFIN. This exchange of an amino acid, which is shared by mammalian GRIFINs, yet does not appear to be detrimental for lactose binding. Considering the pH dependence, contribution to affinity by Glu69 could be reduced by an increasing degree of its protonation. Its pK_a was calculated to be 4.6 so that a loss of enthalpy generation may ensue at this site at low pH. Going above neutral pH, His46 (at pK_a 6.75) may be a factor in the observed affinity decrease at pH 8.5, whose origin appears to be more complex than a single-site alteration.

When extending testing to the 3′-O-sulfated derivative of 2-naphthyl β-lactoside in ITC, the K_D-value decreased from 8.6 to 0.13 μM. This marked enhancement of affinity by presence of the sulfate group is in contrast to 3′-sialylation, as observed in cell binding [19]. When comparing the binding mode of the negatively charged lactose derivative to CG-8N, reported previously [31], with the situation in C-GRIFIN, a lack of interaction with Arg57 and also Glu45 may have an influence on this grading of affinity to the lactoside and its 3′-modified derivatives. Binding-site modeling with the 3′-O-sulfated lactose as ligand provides a set of putative contacts to the sulfate group that can adopt two orientations (Fig. S3). Interestingly, these sets include contacts to Asn48 and Arg50 as well as Trp66, albeit not with the same conformer, as is the case for the N-domains of Gal-4 and -8 [54,55]: Gal-4C, in contrast, appears to employ a transient contact to Trp256 for the slight affinity increase caused by the presence of the 3′-sulfate group [56].

When comparing in detail positions of amino acid of the ligand-free and -loaded subunits of the C-GRIFIN homodimer, one ligand-dependent event of reorganization was revealed (Fig. 6A). The side chain of Arg50 moves toward the glucose ring into the direction of Trp66 from the position of pointing to Asn48, in this place also in crystallographic interactions with Ser54 and Glu78 of a symmetry-related protein. Interestingly, the accommodation of ligand into the N-terminal lectin domain of human Gal-9 triggers such a movement of the side chain of Arg87 to let its NH1 become hydrogen bonded with O2 of the glucose moiety [57]. The movement in C-GRIFIN was also seen in crystals obtained at pH 6.2 (Fig. 6B). When C-GRIFIN in solution bound to lactose on beads and was tryptically fragmented, peptides covering the amino acid stretches of 26–52 and 58–70 had sufficient interactions to maintain their binding during repeated washes and could be eluted [19]. This result is in line with the contact pattern seen in crystals. Taking analysis of C-GRIFIN and lactose binding again to the level of a solution in this report, measuring extent and profile of HDX in the absence and presence of ligand can identify the contact site. Beyond furnishing a sensitive means to do so, measuring the impact of ligand presence on amide deuteration can also detect alterations in this parameter at other sites. This has recently been accomplished for CG-8N when introducing application of this method to galectins [31]. Measured for homodimeric human Gal-1 and CG-1B/2 by small angle neutron scattering and fluorescence correlation spectroscopy, respectively [44,58,59], ligand binding can lead to shape changes into both directions, depending on the type of protein. We thus performed HDX experiments with C-GRIFIN.

3.5. Changes of protein deuteration by presence of ligand

Peptic fingerprinting of C-GRIFIN and sequence coverage is illustrated in Fig. 7 (for complete listing of peptides with sequence assignment, please see Table S1; the N-terminal peptide without release of the methionine, i.e. MALR, is detected in tryptic digests at an overall level of 2.1% together with the predominant ALR tripeptide after release). The number of detected peptides was 94. The size of the panel ensured complete sequence coverage at a redundancy of 7.25. This value denotes the average frequency of a distinct amino acid position covered by the panel of identified peptides. Presence of lactose reduced deuterium uptake into amides, predominantly in the sequence stretch covering canonical amino acids, with strong impact especially on the peptide 55–61 (Fig. 8). Changes seen at position 1–17 and 21–38 should be viewed with caution, because no confirmation by overlapping peptides was possible. The quantitative data on the level of peptides given in Fig. 8 can now be introduced by color coding to the crystal structure. Their implementation into structural models of the binding site is shown in Fig. 6C and D. Accommodation of the binding site by lactose thus reduces extent of deuteration in the region of hydrogen/CH-π bonding, without a marked alteration at other sites.

To pursue the delineation of relative importance of distinct amino acids in this region for ligand binding, site-directed mutagenesis was applied. The example of mammalian Gal-1 had revealed that already the mutation at a single site was sufficient to abolish reactivity to glycans. In detail, the tested cases are Asn46Asp, Arg48His, Asn61Asp, Glu71Gln and Arg73His, the Trp68Leu substitution causing a drastic reduction [60–62]. Interestingly, the natural occurrence of the Arg71Val substitution does obviously not preclude binding of lactose by C-GRIFIN despite the documented reduction in H-bonding to the 6′-hydroxyl group of galactose (Fig. 5). As outlined in the introduction, a mutation can yet have different consequences. Using a histochemical assay to probe lactose-inhibitable reactivity with the pattern of natural glycans in tissue sections, wild-type C-GRIFIN and three mutants were tested.

3.6. Effects of mutations on binding to lactose and tissue sections

The application of tissue sections as assay platform enables to monitor the activity profile of the test proteins with cellular glycoconjugates, covering natural diversity in structural and spatial parameters. In view of the general importance of Trp66's indole ring for C-H/π interactions, as shown in Fig. 5, a Trp66Leu mutant was designed, with the expectation of a substantial loss of signal. Next, the structure of mammalian GRIFIN at position 48 was mimicked by the Asn48Lys mutation. Absence of Asn at the

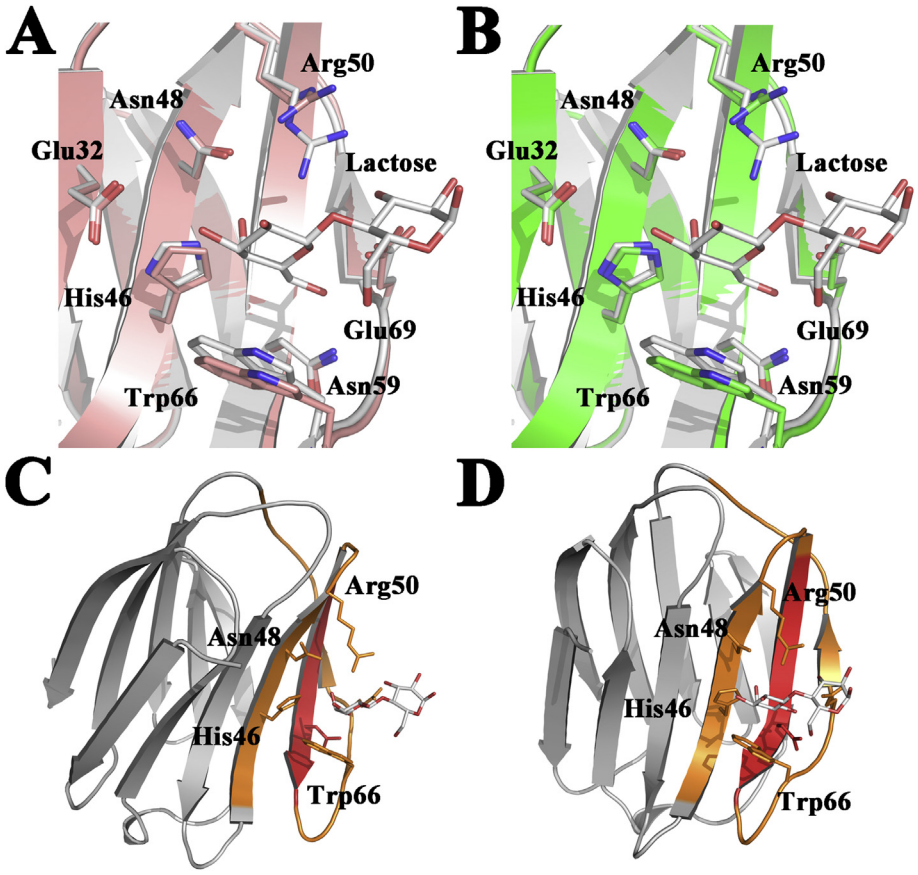

Fig. 6. Superposition of ligand-free (C-atoms in color) and lactose-loaded carbohydrate-binding site architecture of C-GRIFIN at pH 7.5 (A) and pH 6.2 (B). In both cases, please note the change in the position of Arg50 in the presence of ligand. Based on quantitative data of HDX (please see Fig. 8 for details), the three sequence stretches exhibiting reduced deuterium uptake in the presence of lactose are highlighted by coloring (in red for peptide 55–61, showing the highest difference; in brown for peptides 43–54 and 62–78), the C-GRIFIN monomer with the respective regions and amino acids shown from two perspectives (C,D).

Fig. 7. Sequence coverage map of peptic peptides used for HDX experiments. Peptides identified in the mass- spectrometric fingerprinting in the absence and presence of lactose are given as cyan bars set in relation to the amino acid sequence of C-GRIFIN. Alternative cleavage-site usage by pepsin is the origin of the noted redundancy in sequence coverage.

equivalent site leads to knocking down lactose-dependent binding for human Gal-1 noted above. This alteration was combined with an Arg50Val exchange, aimed at further harming hydrogen bonding to the 4′-hydroxyl group of the galactose moiety. Of note, this pair of two sequence deviations is encountered in chicken galectin-related protein that has no affinity for lactose (C-GRP [63]). To complete our series, a triple mutant was engineered. All four variant proteins failed to bind to lactose-bearing beads, precluding

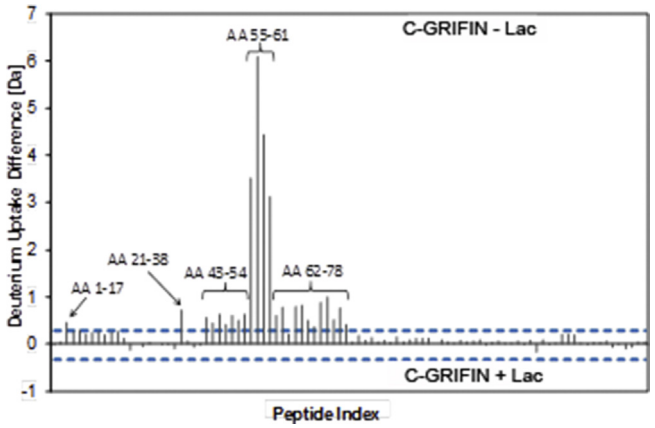

Fig. 8. Ligand-dependent reduction of deuterium uptake in C-GRIFIN. Summary of differences in deuterium uptake over a deuteration time course of 0.5 min, 1 min, 10 min, 60 min and 240 min between peptides of ligand-free and lactose-loaded C-GRIFIN is presented in quantitative form. The peptide index given on the x-axis was calculated on the basis of midpoint values that reflect the position of the peptide within the amino acid sequence of the protein; the blue dotted lines represent the two-sided confidence limit (α 0.02) calculated as described [32].

their purification by standard affinity chromatography, thus requiring the route over fusion-protein design.

In the histochemical assay, the wild-type and the four mutant proteins were tested under identical conditions. Titrations from 4 μg/mL to 48 μg/mL were performed in the absence and presence of 200 mM lactose, flanked by controls to exclude probe-independent staining. Incubation of sections with the wild-type protein led to strong staining that was completely inhibited by the cognate sugar (Fig. 9A). The presence of Trp66Leu mutation decreased signal intensity and capacity of lactose for inhibition (Fig. 9B). In contrast, the substitution at position 48 even increased signal intensity that was not affected by lactose (Fig. 9C). By adding the Arg50Val to the Asn48Lys substitution, signal intensity fell back to the level of the Trp66Leu variant (Fig. 9D). As likewise seen in the case of the triple mutant (not shown), the effect of lactose presence on signal intensity by the double mutant was nearly comparable to that of the Trp66Leu mutant (Fig. 9B,D).

The Asn48Lys substitution, the central difference between mammalian and bird/fish GRIFINs with respect to direct ligand contact, therefore appeared to fundamentally affect relative signal intensity among mutants and susceptibility to presence of lactose. Of course, other alterations present in mammalian GRIFIN, too, could make their presence felt, because reconstitution at three sites of rat GRIFIN (i.e. Val46Phe, Lys47Asn, Val70Arg) did not repair the defect in lectin activity [17]. Furthermore, the examples of long-range effects of the R111H/C2S mutations in human Gal-1, causing a shift in the positions of His52/Trp68 [13], and of the SNP-based Phe19Tyr change in a natural variant of human Gal-8 [64] attest remarkable plasticity and sensitivity for subtle changes. In this respect, it will be very informative to have the crystal structures of CG-3 and also of the C-terminal domain of CG-

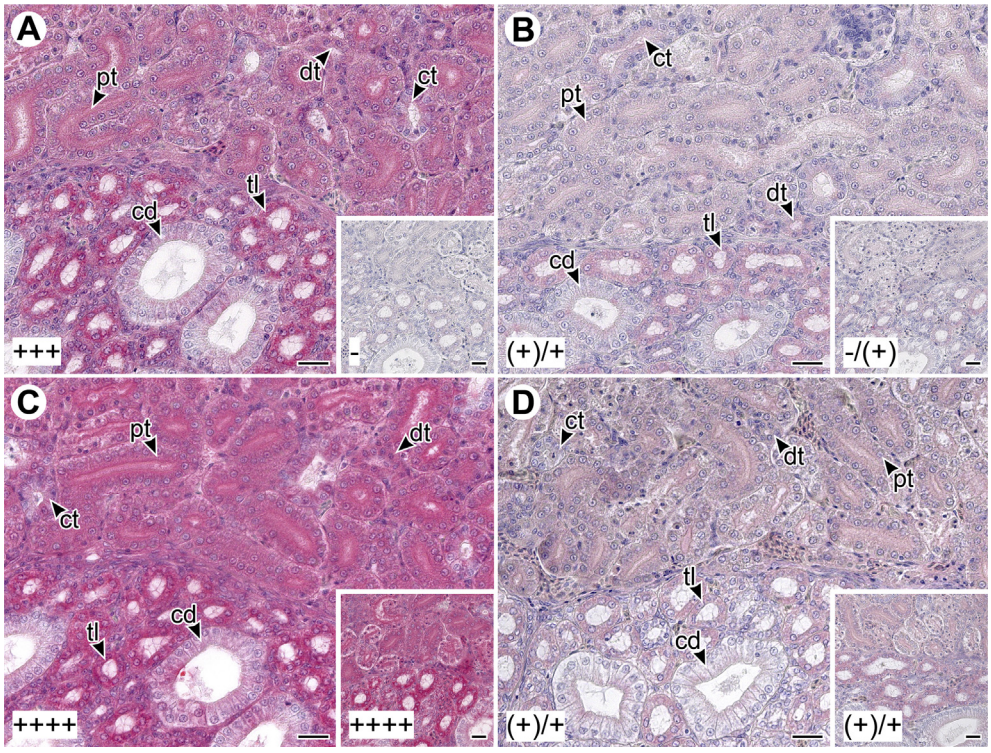

Fig. 9. Histochemical staining profiles of biotinylated wild-type C-GRIFIN and three mutants in paraffin-embedded sections of fixed adult chicken kidney. Wild-type C-GRIFIN strongly stained the thick loops (tl), distal tubules (dt) and the apical part of the proximal tubules (pt) (A). Binding was also detected in the collecting ducts (cd) and in the peripheral collecting tubules (ct). Presence of 200 mM lactose led to complete abolishment of binding of C-GRIFIN (inset to A). The introduction of the Trp66Leu mutation led to marked decrease of staining, with only weak signals in the thick loops (tl), distal tubules (dt) and the collecting tubules (ct) (B). Very weak but significant staining was seen in the proximal tubules (pt). Incubation with 200 mM lactose either slightly reduced signal intensity (thick loops (tl), distal tubules (dt), collecting tubules (ct)) or led to complete inhibition of binding (proximal tubules (pt)) (inset to B). In contrast, the Asn48Lys mutant led to very strong staining (C). No inhibitory effect was seen in the presence of lactose (inset to C). Combining this mutation with an Arg50Val substitution (to obtain the Asn48Lys/Arg50Val double mutant) markedly decreased signal intensity in all areas of the section (D), with no effect by presence of 200 mM lactose (inset to D). The concentration of biotinylated proteins was 12 μg/mL. The corresponding category of signal intensity is given in the bottom left part of each microphotograph, according to the following grading system: -, no staining; (+), very weak but significant staining; +, weak staining; ++, medium-level staining; +++, strong staining; ++++, very strong staining. Scale bars: 20 μm.

8 available, which are closest to C-GRIFIN in the phylogenetic family-tree diagram [19].

The same holds true for the identification of binding partners in the lens. “Since GRIFIN comprises approximately 0.5% of the water-soluble lens protein [17], it is rather remarkable that so little is known about a possible physiological role of this protein in the lens” [35]. In transgenic mouse lenses, chemical cross-linking of a tagged version of human αA-crystallin led to detecting GRIFIN in the complexes, supported by co-elution of the two proteins in gel filtration at a peak around 600 kDa [35]. The K_D-value measured in filtration binding (Scatchard) assays with murine α_L-crystallin was 13.6 ± 5.3 μM (9.4 μM) with a stoichiometry of 0.4 ± 0.08 (0.34) GRIFIN monomer per crystallin monomer (0.25 ± 0.01 for bovine crystallin) [35]. This stoichiometry intimates the possibility that the GRIFIN homodimer may help give order when packaging crystallin proteins. As consequence, GRIFIN's presence contributes to establish the refractive index of the lens.

That galectins of this design have been referred to as “bridging molecules” [65] and can indeed, especially at locally high concentrations, form vesicle aggregates [66–68] or lattices [21] makes them suited to become a molecular “glue” for binding partners [69]. Intriguingly, di- or tetrameric (plant) lectins of the β-sandwich fold are known to assist in ordered packaging. This is an intracellular role of leguminous lectins. Their association to storage proteins destined to fill protein bodies depends either on protein-glycan (for glycosylated vicilin) or protein-protein interactions (for non-glycosylated vicilin and legumin) [70,71]. This dual reactivity is not uncommon, a lectin from slime molds even employing two contact sites for a glycan and for a protein to fulfill its role in ordered cell migration [72]. To take the comparison to GRIFIN further, the leguminous lectins can bind to protein body membranes [73]. The finding of an association of GRIFIN and α-crystallin with the plasma membrane of lens fiber cells [17,74] has led to assuming an influence on “cell elongation and suture formation during lens development” [35]. The homodimeric design as well as high degree of stability and rigidity can thus be molecular means of GRIFINs for helping to build and/or maintain the high-order organization of lens proteins. Bridging of counterreceptors, an often encountered theme in translating glycan-encoded messages by lectins [8,21,75], will in this context likely engender stability of aggregates in three dimensions. Whether and how GRIFINs and their yes/no variability of lectin activity in proteins from different vertebrates actually play a role in these processes remains to be clarified. Equally important, mapping the course of GRIFIN expression and localization in lens development is required to define physiological role(s) of respective proteins with/without lectin activity.

4. Conclusions

The combined analysis of C-GRIFIN in crystals (at seven pH values from 4.2 to 8.5) and in solution (up to 9.0 mg/mL in SAXS) revealed C-GRIFIN to be a stable and compact homodimer with no tendency for aggregation in solution. The contact profile to lactose compensated the Arg71Val deviation and maintained the enthalpically driven nature of binding. Ligand association caused a shift in the position of the side chain of Arg50, the only observed structural change in crystals. In solution, monitoring HDX in peptic fingerprints at 100% sequence coverage, too, confirmed location of the binding site and did not record any significant ligand-dependent change. Localization of contact site(s) for ligands and monitoring for an impact of the association on solvent accessibility of protein regions are the strengths of this technique [31,76]. Implementing the Asn48Lys change, a hallmark of mammalian GRIFINs, made binding of this mutant protein to tissue sections rather insensitive to lactose presence, intimating this position to be a key site for interactions. This result and the presented structural informations build a solid foundation to proceed in the quest to understand GRIFIN's role as lens protein not present, for example, in the retina [17,19,77]. Moreover, they are a step toward completing the structural analysis of the galectin network in a model organism, i.e. in chicken with its seven members.

Conflict of interests

Funding source was not involved in the collection, analysis and interpretation of data, in the writing of the report, and in the decision to submit the article for publication.

Acknowledgments

RR is grateful to the Natural Sciences and Engineering Research Council of Canada (NSERC) for a Canadian Research chair and financial support. AR thanks the Spanish Ministry of Economy and Competitiveness for the financial support through the BFU2016-77835-R project. We are grateful for inspiring discussions with Drs. B. Friday and A. Leddoz, for obtaining access to the ITC equipment to Prof. N. Doucet, to M. Létourneau, J. Gagnon and P.T. Nguyen for helpful advice as well as for the outstanding technical assistance provided by the staff members of the SOLEIL (France) and ALBA (Spain) synchrotrons and for the thorough manuscript review leading to valuable recommendations.

Appendix A. Supplementary data

Supplementary data related to this article can be found at https://doi.org/10.1016/j.biochi.2017.12.003.

References

[1] R. Loris, Principles of structures of animal and plant lectins, Biochim. Biophys. Acta 1572 (2002) 198–208.
[2] D. Solís, N.V. Bovin, A.P. Davis, J. Jiménez-Barbero, A. Romero, R. Roy, K. Smetana Jr., H.-J. Gabius, A guide into glycosciences: how chemistry, biochemistry and biology cooperate to crack the sugar code, Biochim. Biophys. Acta 1850 (2015) 186–235.
[3] J.C. Manning, A. Romero, F.A. Habermann, G. García Caballero, H. Kaltner, H.-J. Gabius, Lectins: a primer for histochemists and cell biologists, Histochem. Cell Biol. 147 (2017) 199–222.
[4] K. Moonens, H. Remaut, Evolution and structural dynamics of bacterial glycan binding adhesins, Curr. Opin. Struct. Biol. 44 (2017) 48–58.
[5] J. Hirabayashi, Recent topics on galectins, Trends Glycosci. Glycotechnol 9 (1997) 1–180.
[6] D.N.W. Cooper, Galectinomics: finding themes in complexity, Biochim. Biophys. Acta 1572 (2002) 209–231.
[7] F.-T. Liu, R.Y. Yang, D.K. Hsu, Galectins in acute and chronic inflammation, Ann. N. Y. Acad. Sci. 1253 (2012) 80–91.
[8] H. Kaltner, S. Toegel, G. García Caballero, J.C. Manning, R.W. Ledeen, H.-J. Gabius, Galectins: their network and roles in immunity/tumor growth control, Histochem. Cell Biol. 147 (2017) 239–256.
[9] S. Saouros, B. Edwards-Jones, M. Reiss, K. Sawmynaden, E. Cota, P. Simpson, T.J. Dowse, U. Jakle, S. Ramboarina, T. Shivarattan, S. Matthews, D. Soldati-Favre, A novel galectin-like domain from *Toxoplasma gondii* micronemal protein 1 assists the folding, assembly, and transport of a cell adhesion complex, J. Biol. Chem. 280 (2005) 38583–38591.
[10] M.H. Huynh, B. Liu, M. Henry, L. Liew, S.J. Matthews, V.B. Carruthers, Structural basis of *Toxoplasma gondii* MIC2-associated protein interaction with MIC2, J. Biol. Chem. 290 (2015) 1432–1441.
[11] G. Peng, D. Sun, K.R. Rajashankar, Z. Qian, K.V. Holmes, F. Li, Crystal structure of mouse coronavirus receptor-binding domain complexed with its murine receptor, Proc. Natl. Acad. Sci. U. S. A. 108 (2011) 10696–10701.
[12] G. Peng, L. Xu, Y.L. Lin, L. Chen, J.R. Pasquarella, K.V. Holmes, F. Li, Crystal structure of bovine coronavirus spike protein lectin domain, J. Biol. Chem. 287 (2012) 41931–41938.
[13] M.F. López-Lucendo, D. Solís, S. André, J. Hirabayashi, K.-i. Kasai, H. Kaltner, H.-J. Gabius, A. Romero, Growth-regulatory human galectin-1: crystallographic characterisation of the structural changes induced by single-site mutations and their impact on the thermodynamics of ligand binding, J. Mol. Biol. 343 (2004) 957–970.
[14] M. Ban, H.J. Yoon, E. Demirkan, S. Utsumi, B. Mikami, F. Yagi, Structural basis of

a fungal galectin from *Agrocybe cylindracea* for recognizing sialoconjugate, J. Mol. Biol. 351 (2005) 695–706.
[15] M. Watanabe, O. Nakamura, K. Muramoto, T. Ogawa, Allosteric regulation of the carbohydrate-binding ability of a novel conger eel galectin by D-mannoside, J. Biol. Chem. 287 (2012) 31061–31072.
[16] M.A. Wälti, P.J. Walser, S. Thore, A. Grunler, M. Bednar, M. Kunzler, M. Aebi, Structural basis for chitotetraose coordination by CGL3, a novel galectin-related protein from *Coprinopsis cinerea*, J. Mol. Biol. 379 (2008) 146–159.
[17] A.T. Ogden, I. Nunes, K. Ko, S. Wu, C.S. Hines, A.F. Wang, R.S. Hegde, R.A. Lang, GRIFIN, a novel lens-specific protein related to the galectin family, J. Biol. Chem. 273 (1998) 28889–28896.
[18] Y. Ueda, C. Fukiage, M. Shih, T.R. Shearer, L.L. David, Mass measurements of C-terminally truncated α-crystallins from two-dimensional gels identify Lp82 as a major endopeptidase in rat lens, Mol. Cell. Proteomics 1 (2002) 357–365.
[19] G. García Caballero, H. Kaltner, M. Michalak, N. Shilova, M. Yegres, S. André, A.K. Ludwig, J.C. Manning, S. Schmidt, M. Schnölzer, N.V. Bovin, D. Reusch, J. Kopitz, H.-J. Gabius, Chicken GRIFIN: a homodimeric member of the galectin network with canonical properties and a unique expression profile, Biochimie 128–129 (2016) 34–47.
[20] H. Ahmed, G.R. Vasta, Unlike mammalian GRIFIN, the zebrafish homologue (DrGRIFIN) represents a functional carbohydrate-binding galectin, Biochem. Biophys. Res. Commun. 371 (2008) 350–355.
[21] N. Sharon, When lectin meets oligosaccharide, Nat. Struct. Biol. 1 (1994) 843–845.
[22] H.-J. Gabius, B. Wosgien, M. Hendrys, A. Bardosi, Lectin localization in human nerve by biochemically defined lectin-binding glycoproteins, neoglycoprotein and lectin-specific antibody, Histochemistry 95 (1991) 269–277.
[23] P. Pernot, A. Round, R. Barrett, A. De Maria Antolinos, A. Gobbo, E. Gordon, J. Huet, J. Kieffer, M. Lentini, M. Mattenet, C. Morawe, C. Mueller-Dieckmann, S. Ohlsson, W. Schmid, J. Surr, P. Theveneau, L. Zerrad, S. McSweeney, Upgraded ESRF BM29 beamline for SAXS on macromolecules in solution, J. Synchrotron Radiat. 20 (2013) 660–664.
[24] D. Franke, D.I. Svergun, DAMMIF, a program for rapid ab-initio shape determination in small-angle scattering, J. Appl. Crystallogr. 42 (2009) 342–346.
[25] V.V. Volkov, D.I. Svergun, Uniqueness of ab initio shape determination in small-angle scattering, J. Appl. Crystallogr. 36 (2003) 860–864.
[26] W. Kabsch, XDS, Acta Crystallogr. D66 (2010) 125–132.
[27] M.D. Winn, C.C. Ballard, K.D. Cowtan, E.J. Dodson, P. Emsley, P.R. Evans, R.M. Keegan, E.B. Krissinel, A.G. Leslie, A. McCoy, S.J. McNicholas, G.N. Murshudov, N.S. Pannu, E.A. Potterton, H.R. Powell, R.J. Read, A. Vagin, K.S. Wilson, Overview of the CCP4 suite and current developments, Acta Crystallogr. D67 (2011) 235–242.
[28] P.D. Adams, P.V. Afonine, G. Bunkoczi, V.B. Chen, I.W. Davis, N. Echols, J.J. Headd, L.W. Hung, G.J. Kapral, R.W. Grosse-Kunstleve, A.J. McCoy, N.W. Moriarty, R. Oeffner, R.J. Read, D.C. Richardson, J.S. Richardson, T.C. Terwilliger, P.H. Zwart, PHENIX: a comprehensive Python-based system for macromolecular structure solution, Acta Crystallogr. D66 (2010) 213–221.
[29] M. Biasini, S. Bienert, A. Waterhouse, K. Arnold, G. Studer, T. Schmidt, F. Kiefer, T. Gallo Cassarino, M. Bertoni, L. Bordoli, T. Schwede, SWISS-MODEL: modelling protein tertiary and quaternary structure using evolutionary information, Nucleic Acids Res. 42 (2014) W252–W258.
[30] P. Emsley, B. Lohkamp, W.G. Scott, K. Cowtan, Features and development of Coot, Acta Crystallogr. D66 (2010) 486–501.
[31] F.M. Ruiz, U. Gilles, I. Lindner, S. André, A. Romero, D. Reusch, H.-J. Gabius, Combining crystallography and hydrogen-deuterium exchange to study galectin-ligand complexes, Chem. Eur. J. 21 (2015) 13558–13568.
[32] D. Houde, S.A. Berkowitz, J.R. Engen, The utility of hydrogen/deuterium exchange mass spectrometry in biopharmaceutical comparability studies, J. Pharm. Sci. 100 (2011) 2071–2086.
[33] H. Kaltner, G. García Caballero, F. Sinowatz, S. Schmidt, J.C. Manning, S. André, H.-J. Gabius, Galectin-related protein: an integral member of the network of chicken galectins. 2. From expression profiling to its immunocyto- and histochemical localization and application as tool for ligand detection, Biochim. Biophys. Acta 1860 (2016) 2298–2312.
[34] R. Roy, Y. Cao, H. Kaltner, N. Kottari, T.C. Shiao, K. Belkhadem, S. André, J.C. Manning, P.V. Murphy, H.-J. Gabius, Teaming up synthetic chemistry and histochemistry for activity screening in galectin-directed inhibitor design, Histochem. Cell Biol. 147 (2017) 285–301.
[35] K.A. Barton, C.D. Hsu, J.M. Petrash, Interactions between small heat shock protein α-crystallin and galectin-related interfiber protein (GRIFIN) in the ocular lens, Biochemistry 48 (2009) 3956–3966.
[36] H. Kaltner, D. Solís, J. Kopitz, M. Lensch, M. Lohr, J.C. Manning, M. Mürnseer, M. Schnölzer, S. André, J.L. Sáiz, H.-J. Gabius, Proto-type chicken galectins revisited: characterization of a third protein with distinctive hydrodynamic behaviour and expression pattern in organs of adult animals, Biochem. J. 409 (2008) 591–599.
[37] F.M. Ruiz, I.S. Fernández, L. López-Merino, L. Lagartera, H. Kaltner, M. Menéndez, S. André, D. Solís, H.-J. Gabius, A. Romero, Fine-tuning of prototype chicken galectins: structure of CG-2 and structure-activity correlations, Acta Crystallogr. D69 (2013) 1665–1676.
[38] P.F. Varela, D. Solís, T. Díaz-Mauriño, H. Kaltner, H.-J. Gabius, A. Romero, The 2.15 Å crystal structure of CG-16, the developmentally regulated homodimeric chicken galectin, J. Mol. Biol. 294 (1999) 537–549.
[39] M.F. López-Lucendo, D. Solís, J.L. Sáiz, H. Kaltner, R. Russwurm, S. André, H.-J. Gabius, A. Romero, Homodimeric chicken galectin CG-1B (C-14): crystal structure and detection of unique redox-dependent shape changes involving inter- and intrasubunit disulfide bridges by gel filtration, ultracentrifugation, site-directed mutagenesis, and peptide mass fingerprinting, J. Mol. Biol. 386 (2009) 366–378.
[40] C.F. Bian, Y. Zhang, H. Sun, D.F. Li, D.C. Wang, Structural basis for distinct binding properties of the human galectins to Thomsen-Friedenreich antigen, PLoS One 6 (2011), e25007.
[41] H.-J. Gabius, H. Kaltner, J. Kopitz, S. André, The glycobiology of the CD system: a dictionary for translating marker designations into glycan/lectin structure and function, Trends Biochem. Sci. 40 (2015) 360–376.
[42] D.M. Freymann, Y. Nakamura, P.J. Focia, R. Sakai, G.T. Swanson, Structure of a tetrameric galectin from *Cinachyrella* sp. (ball sponge), Acta Crystallogr. D68 (2012) 1163–1174.
[43] Y. Nonaka, T. Ogawa, H. Yoshida, H. Shoji, N. Nishi, S. Kamitori, T. Nakamura, Crystal structure of a *Xenopus laevis* skin proto-type galectin, close to but distinct from galectin-1, Glycobiology 25 (2015) 792–803.
[44] L. He, S. André, H.-C. Siebert, H. Helmholz, B. Niemeyer, H.-J. Gabius, Detection of ligand- and solvent-induced shape alterations of cell-growth-regulatory human lectin galectin-1 in solution by small angle neutron and X-ray scattering, Biophys. J. 85 (2003) 511–524.
[45] P.J. Walser, P.W. Haebel, M. Künzler, D. Sargent, U. Kües, M. Aebi, N. Ban, Structure and functional analysis of the fungal galectin CGL2, Structure 12 (2004) 689–702.
[46] D.N. Cooper, R.P. Boulianne, S. Charlton, E.M. Farrell, A. Sucher, B.C. Lu, Fungal galectins, sequence and specificity of two isolectins from *Coprinus cinereus*, J. Biol. Chem. 272 (1997) 1514–1521.
[47] M.F. López-Lucendo, G. Giménez-Gallego, D.N. Cooper, H.-J. Gabius, A. Romero, Gene design, expression, crystallization and preliminary diffraction analysis of two isolectins from the fungus *Coprinus cinereus*: a model for studying functional diversification of galectins in the same organism and their evolutionary pathways, Acta Crystallogr. D60 (2004) 721–724.
[48] M. Nagae, N. Nishi, T. Murata, T. Usui, T. Nakamura, S. Wakatsuki, R. Kato, Crystal structure of the galectin-9 N-terminal carbohydrate recognition domain from *Mus musculus* reveals the basic mechanism of carbohydrate recognition, J. Biol. Chem. 281 (2006) 35884–35893.
[49] V. Krejčiříková, P. Pachl, M. Fábry, P. Malý, P. Rezáčová, J. Brynda, Structure of the mouse galectin-4 N-terminal carbohydrate-recognition domain reveals the mechanism of oligosaccharide recognition, Acta Crystallogr. D67 (2011) 204–211.
[50] H. Ahmed, H.J. Allen, A. Sharma, K.L. Matta, Human splenic galaptin: carbohydrate-binding specificity and characterization of the combining site, Biochemistry 29 (1990) 5315–5319.
[51] R.T. Lee, Y. Ichikawa, H.J. Allen, Y.C. Lee, Binding characteristics of galactoside-binding lectin (galaptin) from human spleen, J. Biol. Chem. 265 (1990) 7864–7871.
[52] G. Levi, V.I. Teichberg, Isolation and physicochemical characterization of electrolectin, a β-D-galactoside-binding lectin from the electric organ of *Electrophorus electricus*, J. Biol. Chem. 256 (1981) 5735–5740.
[53] D. Solís, A. Romero, H. Kaltner, H.-J. Gabius, T. Díaz-Mauriño, Different architecture of the combining sites of two chicken galectins revealed by chemical-mapping studies with synthetic ligand derivatives, J. Biol. Chem. 271 (1996) 12744–12748.
[54] H. Ideo, T. Matsuzaka, T. Nonaka, A. Seko, K. Yamashita, Galectin-8-N-domain recognition mechanism for sialylated and sulfated glycans, J. Biol. Chem. 286 (2011) 11346–11355.
[55] K. Bum-Erdene, H. Leffler, U.J. Nilsson, H. Blanchard, Structural characterisation of human galectin-4 N-terminal carbohydrate recognition domain in complex with glycerol, lactose, 3'-sulfo-lactose, and 2'-fucosyllactose, Sci. Rep. 6 (2016) 20289.
[56] K. Bum-Erdene, H. Leffler, U.J. Nilsson, H. Blanchard, Structural characterization of human galectin-4 C-terminal domain: elucidating the molecular basis for recognition of glycosphingolipids, sulfated saccharides and blood group antigens, FEBS J. 282 (2015) 3348–3367.
[57] D. Solís, M.J. Maté, M. Lohr, J.P. Ribeiro, L. López-Merino, S. André, E. Buzamet, F.J. Cañada, H. Kaltner, M. Lensch, F.M. Ruiz, G. Haroske, U. Wollina, M. Kloor, J. Kopitz, J.L. Sáiz, M. Menéndez, J. Jiménez-Barbero, A. Romero, H.-J. Gabius, N-Domain of human adhesion/growth-regulatory galectin-9: preference for distinct conformers and non-sialylated *N*-glycans and detection of ligand-induced structural changes in crystal and solution, Int. J. Biochem. Cell Biol. 42 (2010) 1019–1029.
[58] A. Göhler, S. André, H. Kaltner, M. Sauer, H.-J. Gabius, S. Doose, Hydrodynamic properties of human adhesion/growth-regulatory galectins studied by fluorescence correlation spectroscopy, Biophys. J. 98 (2010) 3044–3053.
[59] A. Göhler, C. Büchner, S. Doose, H. Kaltner, H.-J. Gabius, Analysis of homodimeric avian and human galectins by two methods based on fluorescence spectroscopy: different structural alterations upon oxidation and ligand binding, Biochimie 94 (2012) 2649–2655.
[60] W.M. Abbott, T. Feizi, Soluble 14-kDa β-galactoside-specific bovine lectin. Evidence from mutagenesis and proteolysis that almost the complete polypeptide chain is necessary for integrity of the carbohydrate recognition domain, J. Biol. Chem. 266 (1991) 5552–5557.
[61] J. Hirabayashi, K.-I. Kasai, Effect of amino acid substitution by sited-directed mutagenesis on the carbohydrate recognition and stability of human 14-kDa β-galactoside-binding lectin, J. Biol. Chem. 266 (1991) 23648–23653.
[62] J. Hirabayashi, K.-I. Kasai, Further evidence by site-directed mutagenesis that

conserved hydrophilic residues form a carbohydrate-binding site of human galectin-1, Glycoconj. J. 11 (1994) 437–442.
[63] G. García Caballero, A. Flores-Ibarra, M. Michalak, N. Khasbiullina, N.V. Bovin, S. André, J.C. Manning, S. Vértesy, F.M. Ruiz, H. Kaltner, J. Kopitz, A. Romero, H.-J. Gabius, Galectin-related protein: an integral member of the network of chicken galectins. 1. From strong sequence conservation of the gene confined to vertebrates to biochemical characteristics of the chicken protein and its crystal structure, Biochim. Biophys. Acta 1860 (2016) 2285–2297.
[64] F.M. Ruiz, B.A. Scholz, E. Buzamet, J. Kopitz, S. André, M. Menéndez, A. Romero, D. Solís, H.-J. Gabius, Natural single amino acid polymorphism (F19Y) in human galectin-8: detection of structural alterations and increased growth-regulatory activity on tumor cells, FEBS J. 281 (2014) 1446–1464.
[65] F.L. Harrison, C.J. Chesterton, Factors mediating cell-cell recognition and adhesion. Galaptins, a recently discovered class of bridging molecules, FEBS Lett. 122 (1980) 157–165.
[66] S. Zhang, R.-O. Moussodia, H.J. Sun, P. Leowanawat, A. Muncan, C.D. Nusbaum, K.M. Chelling, P.A. Heiney, M.L. Klein, S. André, R. Roy, H.-J. Gabius, V. Percec, Mimicking biological membranes with programmable glycan ligands self-assembled from amphiphilic Janus glycodendrimers, Angew. Chem. Int. Ed. 53 (2014) 10899–10903.
[67] S. Zhang, R.-O. Moussodia, C. Murzeau, H.J. Sun, M.L. Klein, S. Vértesy, S. André, R. Roy, H.-J. Gabius, V. Percec, Dissecting molecular aspects of cell interactions using glycodendrimersomes with programmable glycan presentation and engineered human lectins, Angew. Chem. Int. Ed. 54 (2015) 4036–4040.
[68] J. Kopitz, Q. Xiao, A.K. Ludwig, A. Romero, M. Michalak, S.E. Sherman, X. Zhou, C. Dazen, S. Vértesy, H. Kaltner, M.L. Klein, H.-J. Gabius, V. Percec, Reaction of a programmable glycan presentation of glycodendrimersomes and cells with engineered human lectins to show the sugar functionality of the cell surface, Angew. Chem. Int. Ed. 56 (2017) 14677–14681.
[69] K.-i. Kasai, Galectin: intelligent glue, non-bureaucratic bureaucrat or almighty supporting actor, Trends Glycosci. Glycotechnol. 9 (1997) 167–170.
[70] W. Einhoff, G. Fleischmann, T. Freier, H. Kummer, H. Rüdiger, Interactions between lectins and other components of leguminous protein bodies, Biol. Chem. Hoppe Seyler 367 (1986) 15–25.
[71] T. Freier, H. Rüdiger, In vivo binding partners of the *Lens culinaris* lectin, Biol. Chem. Hoppe Seyler 368 (1987) 1215–1223.
[72] H.-J. Gabius, W.R. Springer, S.H. Barondes, Receptor for the cell binding site of discoidin I, Cell 42 (1985) 449–456.
[73] G. Schecher, H. Rüdiger, Interaction of the soybean (*Glycine max*) seed lectin with components of the soybean protein body membrane, Biol. Chem. Hoppe Seyler 375 (1994) 829–832.
[74] B.A. Cobb, J.M. Petrash, Characterization of α-crystallin plasma membrane binding, J. Biol. Chem. 275 (2000) 6664–6672.
[75] H.-J. Gabius, How to crack the sugar code, Folia Biol. (Praha). 63 (2017) 121–131.
[76] D. Kim, H.-M. Lee, K.S. Oh, A.Y. Ki, R.A. Protzman, J.-S. Choi, M.J. Kim, S.H. Kim, B. Vaidya, S.J. Lee, J. Kwon, Exploration of the metal coordination region of concanavalin A for its interaction with human norovirus, Biomaterials 128 (2017) 33–43.
[77] J.C. Manning, G. García Caballero, C. Knospe, H. Kaltner, H.-J. Gabius, Network analysis of adhesion/growth-regulatory galectins and their binding sites in adult chicken retina and choroid, J. Anat. 231 (2017) 23–37.